
E(n) Equivariant Normalizing Flows

Victor Garcia Satorras^{1*}, Emiel Hoogetboom^{1*}, Fabian B. Fuchs²,
Ingmar Posner², Max Welling¹

UvA-Bosch Delta Lab, University of Amsterdam¹,
Department of Engineering Science, University of Oxford²
v.garciasatorras@uva.nl, e.hoogetboom@uva.nl, fabian@robots.ox.ac.uk

Abstract

This paper introduces a generative model equivariant to Euclidean symmetries: E(n) Equivariant Normalizing Flows (E-NFs). To construct E-NFs, we take the discriminative E(n) graph neural networks and integrate them as a differential equation to obtain an invertible equivariant function: a continuous-time normalizing flow. We demonstrate that E-NFs considerably outperform baselines and existing methods from the literature on particle systems such as DW4 and LJ13, and on molecules from QM9 in terms of log-likelihood. To the best of our knowledge, this is the first flow that jointly generates molecule features and positions in 3D.

1 Introduction

Leveraging the structure of the data has long been a core design principle for building neural networks. Convolutional layers for images famously do so by being translation equivariant and therefore incorporating the symmetries of a pixel grid. Analogously, for discriminatory machine learning tasks on 3D coordinate data, taking into account the symmetries of data has significantly improved performance (Thomas et al., 2018; Anderson et al., 2019; Finzi et al., 2020; Fuchs et al., 2020; Klicpera et al., 2020). One might say that equivariance has been proven an effective tool to build inductive bias into the network about the concept of 3D coordinates. However, for generative tasks, e.g., sampling new molecular structures, the development of efficient yet powerful rotation equivariant approaches—while having made great progress—is still in its infancy.

A recent method called E(n) Equivariant Graph Neural Networks (EGNNs) (Satorras et al., 2021) is both computationally cheap and effective in regression and classification tasks for molecular data, while being equivariant to Euclidean symmetries. However, this model is only able to discriminate features on nodes, and cannot generate new molecular structures.

In this paper, we introduce E(n) Equivariant Normalizing Flows (E-NFs): A generative model for E(n) Equivariant data such as molecules in 3D. To construct E-NFs we parametrize a continuous-time flow, where the first-order derivative is modelled by an EGNN. We adapt EGNNs so that they are stable when utilized as a derivative. In addition, we use recent advances in the quantization literature to lift the discrete features of nodes to a continuous space. We show that our proposed flow model significantly outperforms its non-equivariant variants and previous equivariant generative methods (Köhler et al., 2020). Additionally, we apply our method to molecule generation and we show that our method is able to generate realistic molecules when trained on the QM9 dataset.

*Equal contribution.

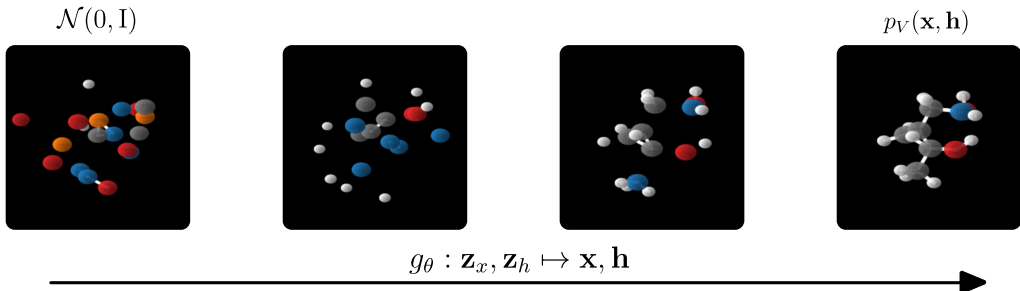


Figure 1: Overview of our method in the sampling direction. An equivariant invertible function g_θ has learned to map samples from a Gaussian distribution to molecules in 3D, described by \mathbf{x}, \mathbf{h} .

2 Background

Normalizing Flows A learnable invertible transformation $\mathbf{x} = g_\theta(\mathbf{z})$ and a simple base distribution p_Z (such as a normal distribution) yield a complex distribution p_X . Let $f_\theta = g_\theta^{-1}$, then the likelihood of a datapoint \mathbf{x} under p_X can be exactly computed using the change of variables formula:

$$p_X(\mathbf{x}) = p_Z(\mathbf{z}) |\det J_f(\mathbf{x})|, \text{ where } \mathbf{z} = f(\mathbf{x}), \quad (1)$$

where J_f is the Jacobian of f_θ . A particular type of normalizing flows are *continuous-time* normalizing flows (Chen et al., 2017, 2018b; Grathwohl et al., 2018). These flows use a conceptual time direction to specify an invertible transformation as a differential equation. The first order differential is predicted by a neural network ϕ , referred to as the dynamics. The continuous-time change of variables formula is given by:

$$\log p_X(\mathbf{x}) = \log p_Z(\mathbf{z}) + \int_0^1 \text{Tr } J_\phi(\mathbf{x}(t)) dt, \text{ where } \mathbf{z} = \mathbf{x} + \int_0^1 \phi(\mathbf{x}(t)) dt, \quad (2)$$

where $\mathbf{x}(0) = \mathbf{x}$ and $\mathbf{x}(1) = \mathbf{z}$. In practice, Chen et al. (2018b); Grathwohl et al. (2018) estimate the trace using Hutchinson’s trace estimator, and the integrals can be straightforwardly computed using the `torchdiffeq` package written by Chen et al. (2018b). It is often desired to regularize the dynamics for faster training and more stable solutions (Finlay et al., 2020). Continuous-time normalizing flows are desirable because the constraints that need to be enforced on ϕ are relatively mild: ϕ only needs to be high order differentiable and Lipschitz continuous, with a possibly large Lipschitz constant.

Equivariance in Normalizing Flows Note that in this context, the desirable property for distributions is often invariance whereas for transformations it is equivariance. Concretely, when a function g_θ is equivariant and a base distribution p_Z is invariant, then the distribution p_X given by $\mathbf{x} = g_\theta(\mathbf{z})$ where $\mathbf{z} \sim p_Z$ is also invariant (Köhler et al., 2020). As a result, one can design expressive invariant distributions using an invariant base distribution p_Z and an equivariant function g_θ . Furthermore, when g_θ is restricted to be bijective and $f_\theta = g_\theta^{-1}$, then equivariance of g_θ implies equivariance of f_θ . In addition, the likelihood p_X can be directly computed using the change of variables formula.

2.1 Equivariance

Equivariance of a function f under a group G is defined as $T_g(f(\mathbf{x})) = f(S_g(\mathbf{x}))$ for all $g \in G$, where S_g, T_g are transformations related to the group element g , where in our case $S_g = T_g$ will be the same. In other words, f being equivariant means that first applying the transformation S_g on x and then f yields the same result as first applying f on x and then transforming using T_g .

In this paper we focus on symmetries of the n -dimensional Euclidean group, referred to as $E(n)$. An important property of this group is that its transformations preserve Euclidean distances. The transformations can be described as rotations, reflections and translations. Specifically, given a set of points $\mathbf{x} = (\mathbf{x}_1, \dots, \mathbf{x}_M) \in \mathbb{R}^{M \times n}$ embedded in an n -dimensional space, an orthogonal matrix $\mathbf{R} \in \mathbb{R}^{n \times n}$ and a translation vector $\mathbf{t} \in \mathbb{R}^n$, we can say f is rotation (and reflection) equivariant if, for $\mathbf{z} = f(\mathbf{x})$ we have $\mathbf{Rz} = f(\mathbf{Rx})$, where \mathbf{Rx} is the shorthand² for $(\mathbf{Rx}_1, \dots, \mathbf{Rx}_M)$. Similarly f

²To be precise, in matrix multiplication notation $(\mathbf{Rx}_1, \dots, \mathbf{Rx}_M) = \mathbf{xR}^T$, for simplicity we use the notation $\mathbf{Rx} = (\mathbf{Rx}_1, \dots, \mathbf{Rx}_M)$ and see \mathbf{R} as an operation instead of a direct multiplication on the entire \mathbf{x} .

is translation equivariant if $\mathbf{z} + \mathbf{t} = f(\mathbf{x} + \mathbf{t})$, where $\mathbf{x} + \mathbf{t}$ is the shorthand for $(\mathbf{x}_1 + \mathbf{t}, \dots, \mathbf{x}_M + \mathbf{t})$. In this work we consider data defined on vertices of a graph $\mathcal{V} = (\mathbf{x}, \mathbf{h})$, which in addition to the position coordinates \mathbf{x} , also includes node features $\mathbf{h} \in \mathbb{R}^{M \times \text{nf}}$ (for example temperature or atom type). Features \mathbf{h} have the property that they are *invariant* to $E(n)$ transformations, while they do affect \mathbf{x} . In other words, rotations and translations of \mathbf{x} do not modify \mathbf{h} . In summary, given a function $f : \mathbf{x}, \mathbf{h} \mapsto \mathbf{z}_x, \mathbf{z}_h$ we require equivariance of f with respect to the Euclidean group $E(n)$ so that for all orthogonal matrices \mathbf{R} and translations \mathbf{t} :

$$\mathbf{R}\mathbf{z}_x + \mathbf{t}, \mathbf{z}_h = f(\mathbf{R}\mathbf{x} + \mathbf{t}, \mathbf{h}) \quad (3)$$

E(n) Equivariant Graph Neural Networks (EGNN) (Satorras et al., 2021) consider a graph $\mathcal{G} = (\mathcal{V}, \mathcal{E})$ with nodes $v_i \in \mathcal{V}$ and edges e_{ij} . Each node v_i is associated with a position vector \mathbf{x}_i and node features \mathbf{h}_i as the ones defined in previous paragraphs. Then, an $E(n)$ Equivariant Graph Convolutional Layer (EGCL) takes as input the set of node embeddings $\mathbf{h}^l = \{\mathbf{h}_0^l, \dots, \mathbf{h}_{M-1}^l\}$, coordinate embeddings $\mathbf{x}^l = \{\mathbf{x}_0^l, \dots, \mathbf{x}_{M-1}^l\}$ at layer l and edge information $\mathcal{E} = (e_{ij})$ and outputs a transformation on \mathbf{h}^{l+1} and \mathbf{x}^{l+1} . Concisely: $\mathbf{h}^{l+1}, \mathbf{x}^{l+1} = \text{EGCL}[\mathbf{h}^l, \mathbf{x}^l, \mathcal{E}]$. This layer satisfies the equivariant constraint defined in Equation 3. The equations that define this layer are the following:

$$\mathbf{m}_{ij} = \phi_e \left(\mathbf{h}_i^l, \mathbf{h}_j^l, \|\mathbf{x}_i^l - \mathbf{x}_j^l\|^2 \right) \quad \text{and} \quad \mathbf{m}_i = \sum_{j \neq i} e_{ij} \mathbf{m}_{ij}, \quad (4)$$

$$\mathbf{x}_i^{l+1} = \mathbf{x}_i^l + \sum_{j \neq i} (\mathbf{x}_i^l - \mathbf{x}_j^l) \phi_x(\mathbf{m}_{ij}) \quad \text{and} \quad \mathbf{h}_i^{l+1} = \phi_h(\mathbf{h}_i^l, \mathbf{m}_i). \quad (5)$$

A neural network $\mathbf{h}^L, \mathbf{x}^L = \text{EGNN}[\mathbf{h}^0, \mathbf{x}^0]$ composed of L layers will define the dynamics of our ODE flow. In our experiments we are not provided with an adjacency matrix, but only node information. Therefore, we use the edge inference module $e_{ij} = \phi_{\text{inf}}(\mathbf{m}_{ij})$ introduced in the EGNN paper that outputs a soft estimation of the edges where $\phi_{\text{inf}} : \mathbb{R}^{\text{nf}} \rightarrow [0, 1]^1$ resembles a linear layer followed by a sigmoid function. This behaves as an attention mechanism over neighbor nodes.

3 Related Work

Group equivariant neural networks (Cohen and Welling, 2016, 2017; Dieleman et al., 2016) have demonstrated their effectiveness in a wide variety of tasks. A growing body of literature is finding neural networks that are equivariant to transformations in Euclidean space (Thomas et al., 2018; Fuchs et al., 2020; Horie et al., 2020; Finzi et al., 2020; Hutchinson et al., 2020; Satorras et al., 2021). These methods have proven their efficacy in discriminative tasks and modelling dynamical systems. On the other hand, graph neural networks (Bruna et al., 2013; Kipf and Welling, 2016) can be seen as networks equivariant to permutations. Often, the methods that study Euclidean equivariance operate on point clouds embedded in Euclidean space, and so they also incorporate permutation equivariance.

Normalizing Flows (Rippel and Adams, 2013; Rezende and Mohamed, 2015; Dinh et al., 2015) are an attractive class of generative models since they admit exact likelihood computation and can be designed for fast inference and sampling. Notably Chen et al. (2018a,b); Grathwohl et al. (2018) introduced continuous-time normalizing flows, a flow that is parametrized via a first-order derivative over time. This class of flows is useful because of the mild constraints on the parametrization function compared to other flow approaches (Dinh et al., 2017; Kingma and Dhariwal, 2018).

There are several specialized methods for molecule generation: Gebauer et al. (2019) generate 3D molecules iteratively via an autoregressive approach, but discretize positions and use additional focus tokens which makes them incomparable in log-likelihood. Gómez-Bombarelli et al. (2016); You et al. (2018); Liao et al. (2019) generate discrete graph structures instead of a coordinate space and Xu et al. (2021) generate molecule positions only. Some flows in literature Noé et al. (2018); Li et al. (2019); Köhler et al. (2020) model positional data, but not in combination with discrete properties.

Recently various forms of normalizing flows for equivariance have been proposed: Köhler et al. (2019, 2020) propose flows for positional data with Euclidean symmetries, Rezende et al. (2019) introduce a Hamiltonian flow which can be designed to be equivariant using an invariant Hamiltonian function. Liu et al. (2019); Biloš and Günnemann (2020) model distributions over graphs, with flows equivariant to permutations. Boyda et al. (2020) introduce equivariant flows for $SU(n)$ symmetries. For adversarial networks, Dey et al. (2021) introduced a generative network equivariant to 90 degree

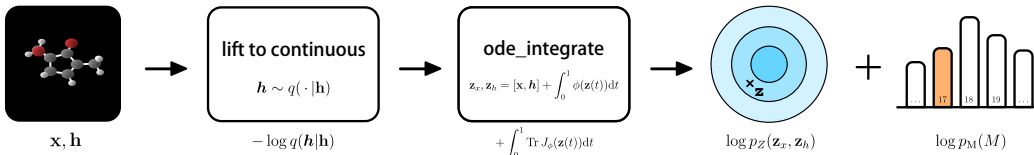


Figure 2: Overview of the training procedure: The discrete \mathbf{h} is lifted to continuous \mathbf{h} . Then the variables \mathbf{x}, \mathbf{h} are transformed by an ODE to $\mathbf{z}_x, \mathbf{z}_h$. To get a lower bound on $\log p_V(\mathbf{x}, \mathbf{h})$ we sum the variational term $-\log q(\mathbf{h}|\mathbf{h})$, the volume term from the ODE $\int_0^1 \text{Tr} J_\phi(\mathbf{z}(t)) dt$, the log-likelihood of the latent representation on a Gaussian $\log p_Z(\mathbf{z}_x, \mathbf{z}_h)$, and the log-likelihood of the molecule size $\log p_M(M)$. To train the model, the sum of these terms is maximized.

image rotations and reflections. Our work differs from these approaches in that we design a general-purpose normalizing flow for sets of nodes that contain both positional *and* invariant features while remaining equivariant to $E(n)$ transformations. This combination of positional and non-positional information results in a more expressive message passing scheme that defines the dynamics of our ODE. A by-product of our general approach is that it also allows us to jointly model features and structure of molecules in 3D space without any additional domain knowledge.

4 Method: $E(n)$ Equivariant Normalizing Flows

In this section we propose our $E(n)$ Equivariant Normalizing Flows, a probabilistic model for data with Euclidean symmetry. The generative process is defined by a simple invariant distribution $p_Z(\mathbf{z}_x, \mathbf{z}_h)$ (such as a Gaussian) over a latent representation of positions $\mathbf{z}_x \in \mathbb{R}^{M \times n}$ and a latent representation of invariant features $\mathbf{z}_h \in \mathbb{R}^{M \times \text{nf}}$ from which an invertible transformation $g_\theta(\mathbf{z}_x, \mathbf{z}_h) = (\mathbf{x}, \mathbf{h})$ generates $\mathcal{V} = (\mathbf{x}, \mathbf{h})$. These nodes consist of node features $\mathbf{h} \in \mathbb{R}^{M \times \text{nf}}$ and position coordinates $\mathbf{x} \in \mathbb{R}^{M \times n}$ embedded in a n -dimensional space. Together, p_Z and g_θ define a distribution p_V over node positions and invariant features.

Since we will restrict g_θ to be invertible, $f_\theta = g_\theta^{-1}$ exists and allows us to map from data space to latent space. This makes it possible to directly optimize the implied likelihood p_V of a datapoint \mathcal{V} utilizing the change of variables formula:

$$p_V(\mathcal{V}) = p_V(\mathbf{x}, \mathbf{h}) = p_Z(f_\theta(\mathbf{x}, \mathbf{h})) |\det J_f| = p_Z(\mathbf{z}_x, \mathbf{z}_h) |\det J_f|, \quad (6)$$

where $J_f = \frac{d(\mathbf{z}_x, \mathbf{z}_h)}{d\mathcal{V}}$ is the Jacobian, where all tensors are vectorized for the Jacobian computation. The goal is to design the model p_V such that translations, rotations and reflections of \mathbf{x} do not change $p_V(\mathbf{x}, \mathbf{h})$, meaning that p_V is $E(n)$ invariant with respect to \mathbf{x} . Additionally, we want p_V to also be invariant to permutations of (\mathbf{x}, \mathbf{h}) . A rich family of distributions can be learned by choosing p_Z to be invariant, and f_θ to be equivariant.

The Normalizing Flow As a consequence, multiple constraints need to be enforced on f_θ . From a probabilistic modelling perspective 1) we require f_θ to be invertible, and from a symmetry perspective 2) we require f_θ to be equivariant. One could utilize the EGNN (Satorras et al., 2021) which is $E(n)$ equivariant, and adapt the transformation so that it is also invertible. The difficulty is that when both these constraints are enforced naively, the space of learnable functions might be small. For this reason we opt for a method that only requires mild constraints to achieve invertibility: neural ordinary differential equations. These methods require functions to be Lipschitz (which most neural networks are in practice, since they operate on a restricted domain) and to be continuously differentiable (which most smooth activation functions are).

To this extent, we define f_θ to be the differential equation, integrated over a conceptual time variable using a differential predicted by the EGNN ϕ . We redefine \mathbf{x}, \mathbf{h} as functions depending on time, where $\mathbf{x}(t=0) = \mathbf{x}$ and $\mathbf{h}(t=0) = \mathbf{h}$ in the data space. Then $\mathbf{x}(1) = \mathbf{z}_x$, $\mathbf{h}(1) = \mathbf{z}_h$ are the latent representations. This admits a formulation of the flow f as the solution to an ODE defined as:

$$\mathbf{z}_x, \mathbf{z}_h = f(\mathbf{x}, \mathbf{h}) = [\mathbf{x}(0), \mathbf{h}(0)] + \int_0^1 \phi(\mathbf{x}(t), \mathbf{h}(t)) dt. \quad (7)$$

The solution to this equation can be straightforwardly obtained by using the `torchdiffeq` package, which also supports backpropagation. The Jacobian term under the ODE formulation is $\log |\det J_f| = \int_0^1 \text{Tr } J_\phi(\mathbf{x}(t), \mathbf{h}(t)) dt$ as explained in Section 2, Equation 2. The Trace of J_ϕ has been approximated with the Hutchinson’s trace estimator.

The Dynamics The dynamics function ϕ in Equation 7 models the first derivatives of \mathbf{x} and \mathbf{h} with respect to time, over which we integrate. Specifically: $\frac{d}{dt}\mathbf{x}(t), \frac{d}{dt}\mathbf{h}(t) = \phi(\mathbf{x}(t), \mathbf{h}(t))$. This derivative is modelled by the EGNN of L layers introduced in Section 2.1:

$$\frac{d}{dt}\mathbf{x}(t), \frac{d}{dt}\mathbf{h}(t) = \mathbf{x}^L(t) - \mathbf{x}(t), \mathbf{h}^L(t) \quad \text{where} \quad \mathbf{x}^L(t), \mathbf{h}^L(t) = \text{EGNN}[\mathbf{x}(t), \mathbf{h}(t)]. \quad (8)$$

Notice that we directly consider the output \mathbf{h}^L from the last layer L of the EGNN as the differential $\frac{d}{dt}\mathbf{h}(t)$ of the node features, since the representation is invariant. In contrast, the differential of the node coordinates is computed as the difference between the EGNN output and input $\frac{d}{dt}\mathbf{x}(t) = \mathbf{x}^L - \mathbf{x}(t)$. This choice is consistent with the nature of velocity-type equivariance: although $\frac{d}{dt}\mathbf{x}(t)$ rotates exactly like \mathbf{x} , it is unaffected by translations as desired.

The original EGNN from (Satorras et al., 2021) is unstable when utilized in an ODE because the coordinate update from Equation 5 would easily explode. Instead, we propose an extension in Equation 9 that normalizes the relative difference of two coordinates by their norm plus a constant C to ensure differentiability. In practice we set $C = 1$ and found this to give stable results.

$$\mathbf{x}_i^{l+1} = \mathbf{x}_i^l + \sum_{j \neq i} \frac{(\mathbf{x}_i^l - \mathbf{x}_j^l)}{\|\mathbf{x}_i^l - \mathbf{x}_j^l\| + C} \phi_x(\mathbf{m}_{ij}) \quad (9)$$

Translation Invariance Recall that we want the distribution $p_V(\mathcal{V})$ to be translation invariant with respect to the overall location and orientation of positional coordinates \mathbf{x} . For simplicity, let’s assume only a distribution $p_X(\mathbf{x})$ over positions and an invertible function $\mathbf{z} = f(\mathbf{x})$. Translation invariance is defined as $p_X(\mathbf{x} + \mathbf{t}) = p_X(\mathbf{x})$ for all \mathbf{t} : a constant function. However, this cannot be a distribution since it cannot integrate to one. Instead, we have to restrict p_X to a subspace.

To construct a translation invariant p_X , we can restrict the data, flow f_θ and prior p_Z to a translation invariant linear subspace, for instance by centering the nodes so that their center of gravity is zero. Then the positions $\mathbf{x} \in \mathbb{R}^{M \times n}$ lie on the $(M - 1) \times n$ -dimensional linear subspace defined by $\sum_{i=1}^M \mathbf{x}_i = \mathbf{0}$. However, from a modelling perspective it is easier to represent node positions as M sets of coordinates that are n -dimensional in the ambient space. In short, we desire the distribution to be defined on the subspace, but with the representation of the nodes in the ambient space.

To limit the flow to the subspace, in practice only the mean of the output of the dynamics network ϕ is removed, following (Köhler et al., 2020). Expanding their analysis, we derive that the Jacobian determinant in the ambient space is indeed equal to the Jacobian determinant in the subspace under this condition. Intuitively, the transformation f_θ does not change orthogonal to the subspace, and as a result there is no volume change in that direction. For this reason the determinant can safely be computed in the ambient space, which conveniently allows the use of existing libraries without modification. Additionally, we can find the proper normalization constant for the base distribution.

For a more formal argument, let P be a $\mathbb{R}^{(M-1) \cdot n \times M \cdot n}$ matrix that projects points to the $(M - 1) \cdot n$ dimensional subspace with orthonormal rows. Consider a collection of points $\mathbf{x} \in \mathbb{R}^{M \times n}$ where $\sum_{i=1}^M \mathbf{x}_i = \mathbf{0}$ and $\mathbf{z} = f_\theta(\mathbf{x})$. Define $\tilde{\mathbf{x}} = P\mathbf{x}$, $\tilde{\mathbf{z}} = P\mathbf{z}$, where \mathbf{x}, \mathbf{z} are considered to be vectorized and $\tilde{\cdot}$ signifies that the variable is defined in the coordinates of the subspace. The Jacobian in the subspace \tilde{J}_f is:

$$\tilde{J}_f = \frac{d\tilde{\mathbf{z}}}{d\tilde{\mathbf{x}}} = \frac{d\tilde{\mathbf{z}}}{d\mathbf{z}} \frac{d\mathbf{z}}{d\mathbf{x}} \frac{d\mathbf{x}}{d\tilde{\mathbf{x}}} = PJ_fP^T. \quad (10)$$

To connect the determinant of J_f to \tilde{J}_f , let $Q \in \mathbb{R}^{M \cdot n \times M \cdot n}$ be the orthogonal extension of P using orthonormal vectors $\mathbf{q}_1, \dots, \mathbf{q}_n$, so that $Q^T = [P^T \ \mathbf{q}_1 \ \dots \ \mathbf{q}_n]$. Then $QJ_fQ^T = \begin{bmatrix} \tilde{J}_f & 0 \\ 0 & I_n \end{bmatrix}$, where $\tilde{J}_f = PJ_fP^T$ and I_n an $n \times n$ identity matrix. From this we observe that $\det J_f = \det QJ_fQ^T = \det \tilde{J}_f$, which proves the claim. As a result of this argument, we are able to utilize existing methods to compute volume changes in the subspace without modification, as $\det \tilde{J}_f = \det J_f$, under the constraint that f_θ is an identity orthogonal to the subspace.

The base distribution Next we need to define a base distribution p_Z . This base distribution can be divided in two parts: the positional part $p(\mathbf{z}_x)$ and the feature part $p(\mathbf{z}_h)$, which we will choose to be independent so that $p(\mathbf{z}_x, \mathbf{z}_h) = p(\mathbf{z}_x) \cdot p(\mathbf{z}_h)$. The feature part is straightforward because the features are already invariant with respect to $E(n)$ symmetries, and only need to be permutation invariant. A common choice is a standard Gaussian $p(\mathbf{z}_h) = \mathcal{N}(\mathbf{z}_h|0, \mathbf{I})$. For the positional part recall that \mathbf{z}_x lies on an $(M-1)n$ subspace, and we need to specify the distribution over this space. Standard Gaussian distributions are reflection and rotation invariant since $\|R\mathbf{z}_x\|^2 = \|\mathbf{z}_x\|^2$ for any rotation or reflection R . Further, observe that for our particular projection $\tilde{\mathbf{z}}_x = P\mathbf{z}_x$ it is true that $\|\tilde{\mathbf{z}}_x\|^2 = \|\mathbf{z}_x\|^2$ since \mathbf{z}_x lies in the subspace. More formally this can be seen using the orthogonal extension Q of P as defined earlier and observing that: $\|\mathbf{z}_x\|^2 = \|Q\mathbf{z}_x\|^2 = \left\| \begin{bmatrix} \tilde{\mathbf{z}}_x \\ \mathbf{0} \end{bmatrix} \right\|^2 = \|\tilde{\mathbf{z}}_x\|^2$. Therefore, a valid choice for a rotation invariant base distribution on the subspace is given by:

$$p(\tilde{\mathbf{z}}_x) = \mathcal{N}(\tilde{\mathbf{z}}_x|0, \mathbf{I}) = \frac{1}{(2\pi)^{(M-1)n/2}} \exp\left(-\frac{1}{2}\|\mathbf{z}_x\|^2\right), \quad (11)$$

which can be directly computed in the ambient space using $\|\mathbf{z}_x\|^2$, with the important property that the normalization constant uses the dimensionality of the subspace: $(M-1)n$, so that the distribution is properly normalized.

Modelling discrete properties Normalizing flows model continuous distributions. However, the node features \mathbf{h} may contain both ordinal (e.g. charge) and categorical (e.g. atom type) features. To train a normalizing flow on these, the values need to be lifted to a continuous space. Let $\mathbf{h} = (\mathbf{h}_{\text{ord}}, \mathbf{h}_{\text{cat}})$ be divided in ordinal and categorical features. For this we utilize variational dequantization (Ho et al., 2019) for the ordinal features and argmax flows (Hoogeboom et al., 2021) for the categorical features. For the ordinal representation \mathbf{h}_{ord} , interval noise $\mathbf{u} \sim q_{\text{ord}}(\cdot|\mathbf{h}_{\text{ord}})$ is used to lift to the continuous representation $\mathbf{h}_{\text{ord}} = \mathbf{h}_{\text{ord}} + \mathbf{u}$. Similarly, \mathbf{h}_{cat} is lifted using a distribution $\mathbf{h}_{\text{cat}} \sim q_{\text{cat}}(\cdot|\mathbf{h}_{\text{cat}})$ where q_{cat} is the probabilistic inverse to an argmax function. Both q_{ord} and q_{cat} are parametrized using normal distributions where the mean and standard deviation are learned using an EGNN conditioned on the discrete representation. This formulation allows training on the continuous representation $\mathbf{h} = (\mathbf{h}_{\text{ord}}, \mathbf{h}_{\text{cat}})$ as it lowerbounds an implied log-likelihood of the discrete representation \mathbf{h} using variational inference:

$$\log p_H(\mathbf{h}) \geq \mathbb{E}_{\mathbf{h} \sim q_{\text{ord}, \text{cat}}(\cdot|\mathbf{h})} \left[\log p_H(\mathbf{h}) - \log q_{\text{ord}, \text{cat}}(\mathbf{h}|\mathbf{h}) \right] \quad (12)$$

To sample the discrete $\mathbf{h} \sim p_H$, first sample the continuous $\mathbf{h} \sim p_H$ via a flow and then compute $\mathbf{h} = (\text{round}(\mathbf{h}_{\text{ord}}), \text{argmax}(\mathbf{h}_{\text{cat}}))$ to obtain the discrete version. In short, instead of training directly on the discrete properties \mathbf{h} , the properties are lifted to the continuous variable \mathbf{h} . The lifting method depends on whether a feature is categorical or ordinal. On this lifted continuous variable \mathbf{h} the flow learns p_H , which is guaranteed to be a lowerbound via Equation 12 on the discrete p_H . To avoid clutter, in the remainder of this paper no distinction is made between \mathbf{h} and \mathbf{h} as one can easily transition between them using $q_{\text{ord}}, q_{\text{cat}}$ and the round, argmax functions.

Finally, the number of nodes M may differ depending on the data. In this case we extend the model using a simple one dimensional categorical distribution p_M of M categories. This distribution p_M is constructed by counting the number of molecules and dividing by the total. The likelihood of a set of nodes is then $p_V(\mathbf{x}, \mathbf{h}, M) = p_{V_M}(\mathbf{x}, \mathbf{h}|M)p_M(M)$, where $p_{V_M}(\mathbf{x}, \mathbf{h}|M)$ is modelled by the flow as before and the same dynamics can be shared for different sizes as the EGNN adapts to the number of nodes. In notation we sometimes omit the M conditioning for clarity. To generate a sample, we first sample $M \sim p_M$, then $\mathbf{z}_x, \mathbf{z}_h \sim p_Z(\mathbf{z}_x, \mathbf{z}_h|M)$ and finally transform to the node features and positions via the flow.

5 Experiments

5.1 DW4 and LJ13

In this section we study two relatively simple systems, DW-4 and LJ-13 presented in (Köhler et al., 2020) where $E(n)$ symmetries are present. These datasets have been synthetically generated by sampling from their respective energy functions using Markov Chain Monte Carlo (MCMC).

DW4: This system consists of only $M=4$ particles embedded in a 2-dimensional space which are governed by an energy function that defines a coupling effect between pairs of particles with multiple metastable states. More details are provided in Appendix A.1.

LJ-13: This is the second dataset used in (Köhler et al., 2020) which is given by the *Leonard-Jones* potential. It is an approximation of inter-molecular pair potentials that models repulsive and attractive interactions. It captures essential physical principles and it has been widely studied to model solid, fluid and gas states. The dataset consists of $M=13$ particles embedded in a 3-dimensional state. More details are provided in Appendix A.1.

Both energy functions (DW4 and LJ13) are equivariant to translations, rotations and reflections which makes them ideal to analyze the benefits of equivariant methods when $E(n)$ symmetries are present on the data. We use the same MCMC generated dataset from (Köhler et al., 2020). For both datasets we use 1,000 validation samples, and 1,000 test samples. We sweep over different numbers of training samples $\{10^2, 10^3, 10^4, 10^5\}$ and $\{10, 10^2, 10^3, 10^4\}$ for DW4 and LJ13 respectively to analyze the performance in different data regimes.

Implementation details: We compare to the state-of-the art $E(n)$ equivariant flows "Simple Dynamics" and "Kernel Dynamics" presented in (Köhler et al., 2020). We also compare to non-equivariant variants of our method, Graph Normalizing Flow (GNF), GNF with attention (GNF-att) and GNF with attention and data augmentation (GNF-att-aug), i.e. augmenting the data with rotations. Our E-NF method and its non-equivariant variants (GNF, GNF-att, GNF-att-aug) consist of 3 layers each, 32 features per layer, and SiLU activation functions. All reported numbers have been averaged over 3 runs. Further implementation details are provided in the Appendix A.1.

Table 1: Negative Log Likelihood comparison on the test partition over different methods on DW4 and LJ13 datasets for different amount of training samples averaged over 3 runs.

# Samples	DW4				LJ13			
	10^2	10^3	10^4	10^5	10	10^2	10^3	10^4
GNF	11.93	11.31	10.38	7.95	43.56	42.84	37.17	36.49
GNF-att	11.65	11.13	9.34	7.83	43.32	36.22	33.84	32.65
GNF-att-aug	8.81	8.31	7.90	7.61	41.09	31.50	30.74	30.93
Simple dynamics	9.58	9.51	9.53	9.47	33.67	33.10	32.79	32.99
Kernel dynamics	8.74	8.67	8.42	8.26	35.03	31.49	31.17	31.25
E-NF	8.31	8.15	7.69	7.48	33.12	30.99	30.56	30.41

Results: In Table 1 we report the cross-validated Negative Log Likelihood for the test partition. Our E-NF outperforms its non-equivariant variants (GNF, GNF-att and GNF-att-aug) and (Köhler et al., 2020) methods in all data regimes. It is interesting to see the significant increase in performance when including data augmentation (from GNF-att to GNF-att-aug) in the non-equivariant models.

5.2 QM9 Positional

We introduce QM9 Positional as a subset of QM9 that only considers positional information and does not encode node features. The aim of this experiment is to compare our method to those that only operate on positional data (Köhler et al., 2020) while providing a more challenging scenario than synthetically generated datasets. QM9 Positional consists only of molecules with 19 atoms/nodes, where each node only has a 3-dimensional positional vector associated. The likelihood of a molecule should be invariant to translations and rotations on a 3-dimensional space which makes equivariant models very suitable for this type of data. The dataset consists of 13,831 training samples, 2,501 for validation and 1,813 for test.

In this experiment, in addition to reporting the estimated Negative Log Likelihood, we designed a a metric to get an additional insight into the quality of the generated samples. More specifically, we produce a histogram of relative distances between all pairs of nodes within each molecule and we

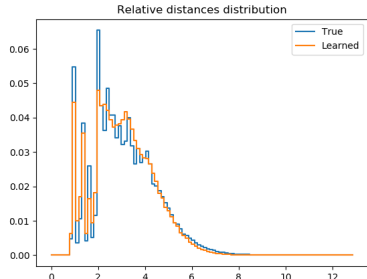


Figure 3: Normalized histogram of relative distances between atoms for QM9 Positional and E-NF generated samples.

compute the Jensen–Shannon divergence (Lin, 1991) $\text{JS}_{\text{div}}(P_{\text{gen}}||P_{\text{data}})$ between the normalized histograms from the generated samples and from the training set. See Figure 3 for an example.

Implementation details: As in the previous experiment, we compare our E-NF to its non-equivariant variants GNF, GNF-att, GNF-att-aug and to the equivariant methods from (Köhler et al., 2020) Simple Dynamics and Kernel Dynamics. The dynamics of our E-NF, GNF, GNF-att and GNF-att-aug consist of 6 convolutional layers each, the number of features is set to 64 and all activation layers are SiLUs. The learning rate is set to $5 \cdot 10^{-4}$ for all experiments except for the E-NF and Simple dynamics which was set to $2 \cdot 10^{-4}$ for stability reasons. All experiments have been trained for 160 epochs. The JS divergence values have been averaged over the last 10 epochs for all models.

# Metrics	NLL	JS(rel. dist)
Simple dynamics	73.0	.086
Kernel dynamics	38.6	.029
GNF	-00.9	.011
GNF-att	-26.6	.007
GNF-att-aug	-33.5	.006
E-NF (ours)	-70.2	.006

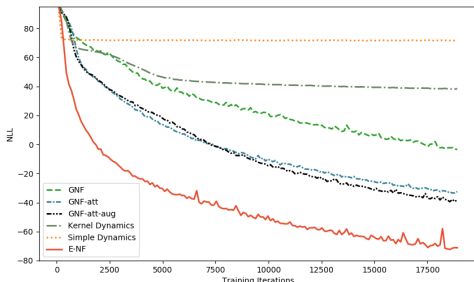


Figure 4: The table on the left presents the Negative Log Likelihood (NLL) $-\log p_V(\mathbf{x})$ for the QM9 Positional dataset on the test data. The figure on the right shows the training curves for all methods.

Results: In the table from Figure 4 we report the cross validated Negative Log Likelihood $-\log p_V(\mathbf{x})$ for the test data and the Jensen-Shannon divergence. Our E-NF outperforms all other algorithms in terms of NLL of the dataset. Additionally, the optimization curve with respect to the number of iterations converges much quicker for our E-NF than for the other methods as shown on the right in Figure 4. Regarding the JS divergence, the E-NF and GNF-att-aug achieve the best performance.

5.3 QM9 Molecules

QM9 (Ramakrishnan et al., 2014) is a molecular dataset standardized in machine learning as a chemical property prediction benchmark. It consists of small molecules (up to 29 atoms per molecule). Atoms contain positional coordinates embedded in a 3D space, a one-hot encoding vector that defines the type of molecule (H, C, N, O, F) and an integer value with the atom charge. Instead of predicting properties from molecules, we use the QM9 dataset to learn a generative distribution over molecules. We desire the likelihood of a molecule to be invariant to translations and rotations, therefore, our $E(n)$ equivariant normalizing flow is very suitable for this task. To summarize, we model a distribution over 3D positions \mathbf{x} , and atom properties \mathbf{h} . These atom properties consist of the atom type (categorical) and atom charge (ordinal).

We use the dataset partitions from (Anderson et al., 2019), 100K/18K/13K for training/validation/test respectively. To train the method, the nodes (\mathbf{x}, \mathbf{h}) are put into Equation 7 as $\mathbf{x}(0), \mathbf{h}(0)$ at time 0 and integrated to time 1. Using the continuous-time change of variables formula and the base distribution, the (negative) log-likelihood of a molecule is computed $-\log p_V(\mathbf{x}, \mathbf{h}, M)$. Since molecules differ in size, this term includes $-\log p_M(M)$ which models the number of atoms as a simple 1D categorical distribution and is part of the generative model as described in Section 4.

Implementation details: We compare our E-NF to the non-equivariant GNF-att and GNF-att-aug introduced in previous experiments. Notice in this experiment we do not compare to (Köhler et al., 2020) since this dataset contains invariant feature data in addition to positional data. Each model is composed of 6 layers, 128 features in the hidden layers and SiLU activation functions. We use the same learning rates as in QM9 Positional. Note that the baselines can be seen as instances of permutation equivariant flows (Liu et al., 2019; Biloš and Günnemann, 2020) but where the GNN architectures have been chosen to be as similar as possible to the architecture in our E-NFs.

Results (quantitative): Results are reported in Table 2. As in previous experiments, our E-NF significantly outperforms the non-equivariant models GNF and GNF-aug. In terms of negative log-likelihood, the E-NF performs much better than its non-equivariant counterparts. One factor that increases this difference is the E-NFs ability to capture the very specific distributions of inter-atomic distances. Since the E-NF is able to better capture these sharp peaks in the distribution, the

Table 2: Neg. log-likelihood $-\log p_V(\mathbf{x}, \mathbf{h}, M)$, atom stability and mol stability for the QM9 dataset.

# Metrics	NLL	Atom stability	Mol stable
GNF-attention	-28.2	72%	0.3%
GNF-attention-augmentation	-29.3	75%	0.5%
E-NF (ours)	-59.7	85%	4.9%
Data	-	99%	95.2%

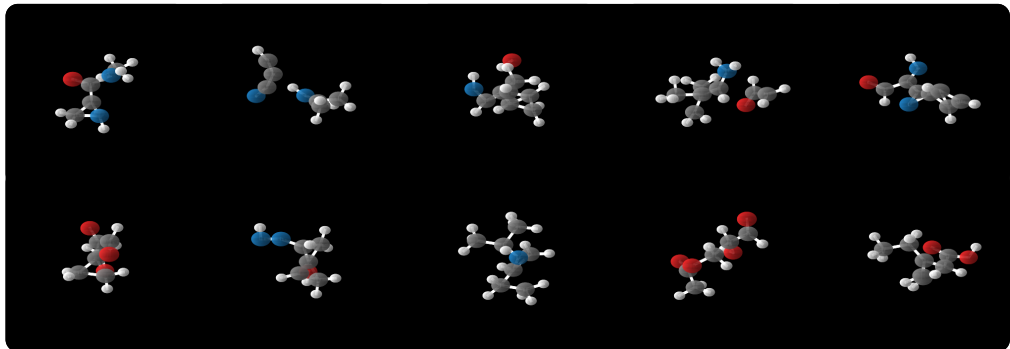


Figure 5: Sampled molecules by our E-NF. The top row contains random samples, the bottom row also contains samples but selected to be stable. Edges are drawn depending on inter-atomic distance.

negative log-likelihood becomes much lower. This effect is also seen when studying the number of stable atoms and molecules, which is very sensitive to the inter-atomic distances. This stability metric was computed over 10,000 samples from the model, for a detailed explanation of stability see Appendix A.3. Observe that it might also be possible to utilize post-processing to increase the molecule stability using prior knowledge. However, here we are mainly using this metric to see how many stable atoms and molecules the E-NF is able to generate in one shot, only by learning the molecule distribution. The E-NF on average produces 85% valid atoms, whereas the best baseline only produces 75% valid atoms. An even stronger improvement is visible when comparing molecule stability: where the E-NF produces 4.9% stable molecules versus 0.5% by the best baseline. Interestingly, the percentage of stable molecules is much lower than that of atoms. This is not unexpected: if even one atom in a large molecule is unstable, the entire molecule is considered to be unstable.

Finally, we evaluate the Validity, Uniqueness and Novelty as defined in (Simonovsky and Komodakis, 2018) for the generated molecules that are stable. For this purpose, we map the 3-dimensional representation of stable molecules to a graph structure and then to a SMILES notation using the rdkit toolkit. All our stable molecules are already defined as valid, therefore we only report the Novelty and Uniqueness since the Validity of those molecules that are already stable is 100%. The Novelty is defined as the ratio of stable generated molecules not present in the training set and Uniqueness is the ratio of unique stable generated molecules. Notice that different generated point clouds in 3-dimensional space may lead to the same molecule in the graph space or SMILES notation. Therefore, even if in the 3D space, all our generated samples were unique and novel, the underlying molecule that they represent doesn't have to be. Using our E-NF, we generated 10,000 examples to compute these metrics. We obtained 491 stable molecules (4.91%), from these subset 99.80% were unique and 93.28% were novel. In a previous version of the paper, these novelty and uniqueness metrics were reported lower due to a bug in the conversion to SMILES notation that has now been fixed in the code. Further analyses are provided in Appendix A.4.

Results (qualitative): In Figure 5 samples from our model are shown. The top row contains random samples that have not been cherry-picked in any way. Note that although the molecule structure is mostly accurate, sometimes small mistakes are visible: Some molecules are disconnected, and some atoms in the molecules do not have the required number of bonds. In the bottom row, random samples have been visualized but under the condition that the sample is stable. Note that atoms might be double-bonded or triple-bonded, which is indicated in the visualization software. For example, in the molecule located in the bottom row 4th column, an oxygen atom is double bonded with the carbon atom at the top of the molecule.

6 Limitations and Conclusions

Limitations In spite of the good results there are some limitations in our model that are worth mentioning and could be addressed in future work: 1) The ODE type of flow makes the training computationally expensive since the same forward operation has to be done multiple times sequentially in order to solve the ODE equation. 2) The combination of the ODE with the EGNN exhibited some instabilities that we had to address (Equation 9). Despite the model being stable in most of the experiments, we still noticed some rare peaks in the loss of the third experiment (QM9) that in one very rare case made it diverge. 3) Different datasets may also contain edge data for which E-NFs should be extended. 4) Our likelihood estimation is invariant to reflections, therefore our model assigns the same likelihood to both a molecule and its mirrored version, which for chiral molecules may not be the same.

Societal Impact Since this work presents a generative model that can be applied to molecular data, it may advance the research at the intersection of chemistry and deep learning. In the long term, more advanced molecule generation methods can benefit applications in drug research and material discovery. Those long term applications may have a positive impact in society, for example, creating new medications or designing new catalyst materials that permit cheaper production of green energy. Negative implications of our work may be possible when molecules or materials are created for immoral purposes, such as the creation of toxins or illegal drugs.

Conclusions In this paper we have introduced $E(n)$ Equivariant Normalizing Flows (E-NFs): A generative model equivariant to Euclidean symmetries. E-NFs are continuous-time normalizing flows that utilize an EGNN with improved stability as parametrization. We have demonstrated that E-NFs considerably outperform existing normalizing flows in log-likelihood on DW4, LJ13, QM9 and also in the stability of generated molecules and atoms.

References

- Anderson, B., Hy, T.-S., and Kondor, R. (2019). Cormorant: Covariant molecular neural networks. *arXiv preprint arXiv:1906.04015*.
- Biloš, M. and Günnemann, S. (2020). Equivariant normalizing flows for point processes and sets. *arXiv preprint arXiv:2010.03242*.
- Boyd, D., Kanwar, G., Racanière, S., Rezende, D. J., Albergo, M. S., Cranmer, K., Hackett, D. C., and Shanahan, P. E. (2020). Sampling using $SU(N)$ gauge equivariant flows. *CoRR*, abs/2008.05456.
- Bruna, J., Zaremba, W., Szlam, A., and LeCun, Y. (2013). Spectral networks and locally connected networks on graphs. *arXiv preprint arXiv:1312.6203*.
- Chen, C., Li, C., Chen, L., Wang, W., Pu, Y., and Carin, L. (2017). Continuous-time flows for deep generative models. *arXiv preprint arXiv:1709.01179*.
- Chen, C., Li, C., Chen, L., Wang, W., Pu, Y., and Carin, L. (2018a). Continuous-time flows for efficient inference and density estimation. In Dy, J. G. and Krause, A., editors, *Proceedings of the 35th International Conference on Machine Learning, ICML*.
- Chen, T. Q., Rubanova, Y., Bettencourt, J., and Duvenaud, D. K. (2018b). Neural ordinary differential equations. In *Advances in Neural Information Processing Systems*, pages 6572–6583.
- Cohen, T. and Welling, M. (2016). Group equivariant convolutional networks. In Balcan, M. and Weinberger, K. Q., editors, *Proceedings of the 33rd International Conference on Machine Learning, ICML*.
- Cohen, T. S. and Welling, M. (2017). Steerable cnns. In *5th International Conference on Learning Representations, ICLR*.
- Dey, N., Chen, A., and Ghafurian, S. (2021). Group equivariant generative adversarial networks. In *International Conference on Learning Representations*.

- Dieleman, S., Fauw, J. D., and Kavukcuoglu, K. (2016). Exploiting cyclic symmetry in convolutional neural networks. In Balcan, M. and Weinberger, K. Q., editors, *Proceedings of the 33rd International Conference on Machine Learning, ICML*, volume 48, pages 1889–1898. JMLR.org.
- Dinh, L., Krueger, D., and Bengio, Y. (2015). NICE: Non-linear independent components estimation. *3rd International Conference on Learning Representations, ICLR, Workshop Track Proceedings*.
- Dinh, L., Sohl-Dickstein, J., and Bengio, S. (2017). Density estimation using Real NVP. *5th International Conference on Learning Representations, ICLR*.
- Finlay, C., Jacobsen, J., Nurbekyan, L., and Oberman, A. M. (2020). How to train your neural ODE: the world of jacobian and kinetic regularization. In *Proceedings of the 37th International Conference on Machine Learning, ICML*.
- Finzi, M., Stanton, S., Izmailov, P., and Wilson, A. G. (2020). Generalizing convolutional neural networks for equivariance to lie groups on arbitrary continuous data. In *Proceedings of the 37th International Conference on Machine Learning, ICML*.
- Fuchs, F. B., Worrall, D. E., Fischer, V., and Welling, M. (2020). Se(3)-transformers: 3d rotation equivariant attention networks. *CoRR*, abs/2006.10503.
- Gebauer, N. W. A., Gastegger, M., and Schütt, K. (2019). Symmetry-adapted generation of 3d point sets for the targeted discovery of molecules. In *Advances in Neural Information Processing Systems 32: Annual Conference on Neural Information Processing Systems 2019, NeurIPS*.
- Gómez-Bombarelli, R., Duvenaud, D., Hernández-Lobato, J. M., Aguilera-Iparraguirre, J., Hirzel, T. D., Adams, R. P., and Aspuru-Guzik, A. (2016). Automatic chemical design using a data-driven continuous representation of molecules. *CoRR*, abs/1610.02415.
- Grathwohl, W., Chen, R. T., Bettencourt, J., Sutskever, I., and Duvenaud, D. (2018). Ffjord: Free-form continuous dynamics for scalable reversible generative models. *arXiv preprint arXiv:1810.01367*.
- Ho, J., Chen, X., Srinivas, A., Duan, Y., and Abbeel, P. (2019). Flow++: Improving flow-based generative models with variational dequantization and architecture design. *36th International Conference on Machine Learning*.
- Hooeboom, E., Nielsen, D., Jaini, P., Forré, P., and Welling, M. (2021). Argmax flows and multinomial diffusion: Towards non-autoregressive language models. *CoRR*, abs/2102.05379.
- Horie, M., Morita, N., Ihara, Y., and Mitsume, N. (2020). Isometric transformation invariant and equivariant graph convolutional networks. *CoRR*, abs/2005.06316.
- Hutchinson, M., Lan, C. L., Zaidi, S., Dupont, E., Teh, Y. W., and Kim, H. (2020). Lietransformer: Equivariant self-attention for lie groups. *CoRR*, abs/2012.10885.
- Kingma, D. P. and Dhariwal, P. (2018). Glow: Generative flow with invertible 1x1 convolutions. In *Advances in Neural Information Processing Systems*, pages 10236–10245.
- Kipf, T. N. and Welling, M. (2016). Semi-supervised classification with graph convolutional networks. *arXiv preprint arXiv:1609.02907*.
- Klicpera, J., Groß, J., and Günnemann, S. (2020). Directional message passing for molecular graphs. In *8th International Conference on Learning Representations, ICLR 2020, Addis Ababa, Ethiopia, April 26-30, 2020*. OpenReview.net.
- Köhler, J., Klein, L., and Noé, F. (2019). Equivariant flows: sampling configurations for multi-body systems with symmetric energies. *CoRR*, abs/1910.00753.
- Köhler, J., Klein, L., and Noé, F. (2020). Equivariant flows: Exact likelihood generative learning for symmetric densities. In *Proceedings of the 37th International Conference on Machine Learning, ICML 2020, 13-18 July 2020, Virtual Event*, volume 119 of *Proceedings of Machine Learning Research*, pages 5361–5370. PMLR.
- Li, S., Dong, C., Zhang, L., and Wang, L. (2019). Neural canonical transformation with symplectic flows. *CoRR*, abs/1910.00024.

- Liao, R., Li, Y., Song, Y., Wang, S., Hamilton, W. L., Duvenaud, D., Urtasun, R., and Zemel, R. S. (2019). Efficient graph generation with graph recurrent attention networks. In *Advances in Neural Information Processing Systems 32: Annual Conference on Neural Information Processing Systems 2019, NeurIPS*.
- Lin, J. (1991). Divergence measures based on the shannon entropy. *IEEE Transactions on Information theory*, 37(1):145–151.
- Liu, J., Kumar, A., Ba, J., Kiros, J., and Swersky, K. (2019). Graph normalizing flows. *arXiv preprint arXiv:1905.13177*.
- Nielsen, D., Jaini, P., Hoogeboom, E., Winther, O., and Welling, M. (2020). Survae flows: Surjections to bridge the gap between vaes and flows. *CoRR*, abs/2007.02731.
- Noé, F., Olsson, S., and Wu, J. K. H. (2018). Boltzmann generators - sampling equilibrium states of many-body systems with deep learning. *CoRR*, abs/1812.01729.
- Nwankpa, C., Ijomah, W., Gachagan, A., and Marshall, S. (2018). Activation functions: Comparison of trends in practice and research for deep learning. *arXiv preprint arXiv:1811.03378*.
- Ramakrishnan, R., Dral, P. O., Rupp, M., and Von Lilienfeld, O. A. (2014). Quantum chemistry structures and properties of 134 kilo molecules. *Scientific data*, 1(1):1–7.
- Rezende, D. and Mohamed, S. (2015). Variational Inference with Normalizing Flows. In *Proceedings of the 32nd International Conference on Machine Learning*, volume 37 of *Proceedings of Machine Learning Research*, pages 1530–1538. PMLR.
- Rezende, D. J., Racanière, S., Higgins, I., and Toth, P. (2019). Equivariant hamiltonian flows. *CoRR*, abs/1909.13739.
- Rippel, O. and Adams, R. P. (2013). High-dimensional probability estimation with deep density models. *arXiv preprint arXiv:1302.5125*.
- Satorras, V. G., Hoogeboom, E., and Welling, M. (2021). E (n) equivariant graph neural networks. *arXiv preprint arXiv:2102.09844*.
- Simonovsky, M. and Komodakis, N. (2018). Graphvae: Towards generation of small graphs using variational autoencoders. In *International conference on artificial neural networks*, pages 412–422. Springer.
- Thomas, N., Smidt, T., Kearnes, S., Yang, L., Li, L., Kohlhoff, K., and Riley, P. (2018). Tensor field networks: Rotation-and translation-equivariant neural networks for 3d point clouds. *arXiv preprint arXiv:1802.08219*.
- Xu, M., Luo, S., Bengio, Y., Peng, J., and Tang, J. (2021). Learning neural generative dynamics for molecular conformation generation. *CoRR*, abs/2102.10240.
- You, J., Ying, R., Ren, X., Hamilton, W. L., and Leskovec, J. (2018). Graphrnn: Generating realistic graphs with deep auto-regressive models. In Dy, J. G. and Krause, A., editors, *Proceedings of the 35th International Conference on Machine Learning, ICML*.

A Experiment details

In this Appendix section we provide more details about the implementation of the experiments. First we introduce those parts of the model architecture that are the same across all experiments. The EGNN module defined in Section 2.1, Equations 4 and 5 is composed of four Multilayer Perceptrons (MLPs) ϕ_e , ϕ_x , ϕ_h and ϕ_{inf} . We used the same design from the original EGNN paper (Satorras et al., 2021) for all MLPs except for ϕ_x . The description of the modules would be as follows:

- ϕ_e (edge operation): consists of a two-layer MLP with two SiLU (Nwankpa et al., 2018) activation functions that takes as input $(\mathbf{h}_i, \mathbf{h}_j, \|\mathbf{x}_i - \mathbf{x}_j\|^2)$ and outputs the edge embedding \mathbf{m}_{ij} .
- ϕ_x (coordinate operation): consists of a two layers MLP with a SiLU activation function in its hidden layer and a Tanh activation function at the output layer. It takes as input the edge embedding \mathbf{m}_{ij} and outputs a scalar value.
- ϕ_h (node operation): consists of a two layers MLP with one SiLU activation function in its hidden layer and a residual connection: $[\mathbf{h}_i^l, \mathbf{m}_i] \rightarrow \{\text{Linear}() \rightarrow \text{SiLU}() \rightarrow \text{Linear}() \rightarrow \text{Addition}(\mathbf{h}_i^l)\} \rightarrow \mathbf{h}_i^{l+1}$.
- ϕ_{inf} (edge inference operation): Consists of a Linear layer followed by a Sigmoid layer that takes as input the edge embedding \mathbf{m}_{ij} and outputs a scalar value.

These functions define our E(n) Equivariant Flow dynamics (E-NF), the Graph Normalizing Flow dynamics (GNF), Graph Normalizing Flow with attention (GNF-att) and Graph Normalizing Flow with attention and data augmentation (GNF-att-aug). The variations regarding architectural choices among experiments are the number of layers and hidden features per layer. In the following we explicitly write down the dynamics used for the ENF, GNF, GNF-att and GNF-att-aug baselines.

- E-NF (Dynamics): We can write the ENF dynamics introduced in Section 2.1 adapted for our method in Section 4 as:

$$\mathbf{m}_{ij} = \phi_e \left(\mathbf{h}_i^l, \mathbf{h}_j^l, \|\mathbf{x}_i^l - \mathbf{x}_j^l\|^2 \right) \quad (13)$$

$$\mathbf{x}_i^{l+1} = \mathbf{x}_i^l + \sum_{j \neq i} \frac{(\mathbf{x}_i^l - \mathbf{x}_j^l)}{\|\mathbf{x}_i^l - \mathbf{x}_j^l\| + 1} \phi_x(\mathbf{m}_{ij}) \quad (14)$$

$$\mathbf{m}_i = \sum_{j \neq i} \phi_{\text{inf}}(\mathbf{m}_{ij}) \mathbf{m}_{ij}, \quad (15)$$

$$\mathbf{h}_i^{l+1} = \phi_h(\mathbf{h}_i^l, \mathbf{m}_i) \quad (16)$$

- GNF: The dynamics for this method are a standard Graph Neural Network which can also be interpreted as a variant of the EGNN with no equivariance. The dataset coordinates \mathbf{x} are treated as \mathbf{h} features, therefore they are provided as input to \mathbf{h}^0 through a linear mapping before its first layer. Since our datasets do not consider adjacency matrices we let $e_{ij} = 1$ for all ij .

$$\mathbf{m}_{ij} = \phi_e(\mathbf{h}_i^l, \mathbf{h}_j^l) \quad (17)$$

$$\mathbf{m}_i = \sum_{j \neq i} e_{ij} \mathbf{m}_{ij}, \quad (18)$$

$$\mathbf{h}_i^{l+1} = \phi_h(\mathbf{h}_i^l, \mathbf{m}_i) \quad (19)$$

- GNF-att: This model is almost the same as GNF with the only difference that it infers the edges through $e_{ij} = \phi_{\text{inf}}(\mathbf{m}_{ij})$ which can also be seen as a form of attention.
- GNF-att-aug: This is the exact same model as GNF-att. The only difference lies in the pre-processing of the data since we perform data augmentation by rotating the node positions before inputting them to the model.

A.1 DW4 and LJ13 experiments

In the following we report the DW4 (equation 20) and LJ13 (equation 21) energy functions introduced in (Köhler et al., 2020):

$$u^{\text{DW}}(x) = \frac{1}{2\tau} \sum_{i,j} a (d_{ij} - d_0) + b (d_{ij} - d_0)^2 + c (d_{ij} - d_0)^4 \quad (20)$$

$$u^{\text{LJ}}(x) = \frac{\epsilon}{2\tau} \left[\sum_{i,j} \left(\left(\frac{r_m}{d_{ij}} \right)^{12} - 2 \left(\frac{r_m}{d_{ij}} \right)^6 \right) \right] \quad (21)$$

Where $d_{ij} = \|\mathbf{x}_i - \mathbf{x}_j\|$ is the distance between two particles. The design parameters a, b, c, d and temperature τ from DW4 and the design parameters ϵ, r_m and τ from LJ13 are the same ones used in (Köhler et al., 2020).

Implementation details All methods are trained with the Adam optimizer, weight decay 10^{-12} , batch size 100, the learning rate was tuned independently for each method which resulted in 10^{-3} for all methods except for the E-NF model which was $5 \cdot 10^{-4}$.

In tables 3 and 4 we report the same DW4 and LJ13 averaged results from Section 5.1 but including the standard deviations over the three runs.

Table 3: Negative Log Likelihood comparison on the test partition of DW4 dataset for different amount of training samples. Averaged over 3 runs and including standard deviations.

# Samples	DW4			
	10^2	10^3	10^4	10^5
GNF	11.93 ± 0.41	11.31 ± 0.07	10.38 ± 0.11	7.95 ± 0.17
GNF-att	11.65 ± 0.39	11.13 ± 0.38	9.34 ± 0.29	7.83 ± 0.15
GNF-att-aug	8.81 ± 0.23	8.31 ± 0.19	7.90 ± 0.04	7.61 ± 0.06
Simple dynamics	9.58 ± 0.05	9.51 ± 0.01	9.53 ± 0.02	9.47 ± 0.06
Kernel dynamics	8.74 ± 0.02	8.67 ± 0.01	8.42 ± 0.00	8.26 ± 0.03
E-NF	8.31 ± 0.05	8.15 ± 0.10	7.69 ± 0.06	7.48 ± 0.05

Table 4: Negative Log Likelihood comparison on the test partition of LJ13 dataset for different amount of training samples. Averaged over 3 runs and including standard deviations.

# Samples	LJ13			
	10	10^2	10^3	10^4
GNF	43.56 ± 0.79	42.84 ± 0.52	37.17 ± 1.79	36.49 ± 0.81
GNF-att	43.32 ± 0.20	36.22 ± 0.34	33.84 ± 1.60	32.65 ± 0.57
GNF-att-aug	41.09 ± 0.53	31.50 ± 0.35	30.74 ± 0.86	30.93 ± 0.73
Simple dynamics	33.67 ± 0.07	33.10 ± 0.10	32.79 ± 0.13	32.99 ± 0.11
Kernel dynamics	35.03 ± 0.48	31.49 ± 0.06	31.17 ± 0.05	31.25 ± 0.12
E-NF	33.12 ± 0.85	30.99 ± 0.95	30.56 ± 0.35	30.41 ± 0.16

A.2 QM9 Positional and QM9

Both experiments QM9 and QM9 positional have been trained with batch size 128 and weight decay 10^{-12} . The learning rate was set to $5 \cdot 10^{-4}$ for all methods except for the E-NF and Simple dynamics where it was reduced to $2 \cdot 10^{-12}$.

The flows trained on QM9 have all been trained for 30 epochs. Training these models takes approximately 2 weeks using two NVIDIA 1080Ti GPUs. The flows trained on QM9 Positional have been trained for 160 epochs in single NVIDIA 1080Ti GPUs. Simple Dynamics would train in less than a day, Kernel Dynamics around 2 days, the other methods can take up to 7 days. The training of the models becomes slower per epoch as the performance improves, due to the required steps in the ODE solver. For QM9, the model performance is averaged over 3 test set passes, where variance originates from dequantization and the trace estimator, see Table 5.

Table 5: Neg. log-likelihood averaged over 3 passes, variance from dequantization and trace estimator.

	NLL
GNF-attention	-28.2 ± 0.49
GNF-attention-augmentation	-29.3 ± 0.02
E-NF (ours)	-59.7 ± 0.12

A.3 Stability of Molecules Benchmark

In the QM9 experiment, we also report the % of stable molecules and atoms. This section explains how we test for molecule stability. In addition, we explain why there is not a set of rules that will judge *every* molecule in the dataset stable. First of all, we say that an atom is stable when the number of bonds with other atoms matches their valence. For the atoms used their respective valencies are (H: 1, C: 4, N: 3, O: 2, F: 1). A molecule is stable when *all* of its atoms are stable. The most straightforward method to decide whether atoms are bonded is to compare their relative distance. There are some limitations to this method. For instance, QM9 contains snapshots of molecules in a single configuration, and in reality atoms of a molecule are constantly in motion. In addition, the type of molecule can also greatly influence the relative distances, for instance due to collisions, the Van der Waals force and inter-molecule Hydrogen bonds. Further, environmental circumstances such as pressure and temperature may also affect bond distance. For these reasons it is not possible to design a distance based rule that considers every molecule in QM9 stable, based only on a snapshot. To find the most optimal rules for QM9, we tune the average bond distance for every atom-type pair to achieve the highest molecule stability on QM9 on the train set with results in 95.3% stable molecules and 99% stable atoms. On the test set these rules result in 95.2% stable molecules and 99% stable atoms.

The specific distances that we used to define the types of bond (SINGLE, DOUBLE TRIPLE or NONE) are available in the code and were obtained from http://www.wiredchemist.com/chemistry/data/bond_energies_lengths.html. Notice the type of bond depends on the type of atoms that form that bond and the relative distance among them. Therefore, given a conformation of atoms, we deterministically compute the bonds among all pairs of atoms. Then we say an atom is stable if its number of bonds with other atoms matches its valence.

A.4 Further QM9 analysis | Validity, Uniqueness, Novelty

Validity is defined as the ratio of molecules that are valid from all the generated ones. *Uniqueness* is defined as the number of valid generated molecules that are unique divided by the number of all valid generated molecules. *Novelty* is defined as the number of valid generated molecules that are not part of the training set divided by the total number of valid generated molecules. In our case, all stable molecules are valid, therefore, we only report the Uniqueness and Novelty. Absolute and percentage values are reported when generating 10.000 examples. Metrics have been computed as in (Simonovsky and Komodakis, 2018) with rdkit <https://www.rdkit.org/>.

In addition to the previous metrics, in Figure 6, we plot a histogram of the number of atoms per molecule and also of the type of atoms for both the stable generated molecules and the ground truth ones.

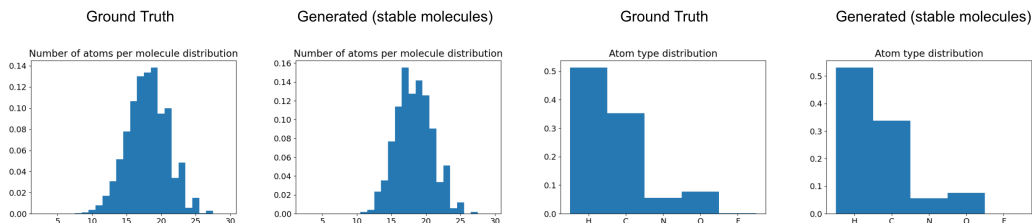


Figure 6: Number of atoms per molecule distributions and atom type distribution for the stable generated molecules and the training (ground truth) molecules.

B Lifting Discrete Features to Continuous Space

In this section additional details are discussed describing how discrete variables are lifted to a continuous space. As in the main text, we let $\mathbf{h} = (\mathbf{h}_{\text{ord}}, \mathbf{h}_{\text{cat}})$ be the discrete features on the nodes, either ordinal or categorical. For simplicity we can omit the number of nodes and even the number of feature dimensions. Then $\mathbf{h}_{\text{ord}} \in \mathbb{Z}$ and $\mathbf{h}_{\text{cat}} \in \mathbb{Z}$. Note here that although the representation for \mathbf{h}_{ord} and \mathbf{h}_{cat} are the same, they are treated differently because of their ordinal or categorical nature.

Now let $\mathbf{h} = (\mathbf{h}_{\text{ord}}, \mathbf{h}_{\text{cat}})$ be its continuous counterpart. We will utilize variational dequantization (Ho et al., 2019) for the ordinal features. In this framework mapping \mathbf{h}_{ord} to \mathbf{h}_{ord} can be done via rounding (down) so that $\mathbf{h}_{\text{ord}} = \text{round}(\mathbf{h}_{\text{ord}})$. Similarly we will utilize argmax flows (Hoogeboom et al., 2021) to map the categorical map which amounts to $\mathbf{h}_{\text{cat}} = \text{argmax}(\mathbf{h}_{\text{cat}})$. Here $\mathbf{h}_{\text{ord}} \in \mathbb{R}$ and $\mathbf{h}_{\text{cat}} \in \mathbb{R}^K$ where K is the number of classes.

The transformation $\mathbf{h} \mapsto \mathbf{h}$ given by $\mathbf{h} = (\text{round}(\mathbf{h}_{\text{ord}}), \text{argmax}(\mathbf{h}_{\text{cat}}))$ is completely deterministic, and to derive our objective later we can formalize this as a distribution with all probability mass on a single event: $P(\mathbf{h}|\mathbf{h}) = \mathbb{1}[\mathbf{h} = (\text{round}(\mathbf{h}_{\text{ord}}), \text{argmax}(\mathbf{h}_{\text{cat}}))]$ as done in (Nielsen et al., 2020). Then the (discrete) generative model $p_H(\mathbf{h}) = \mathbb{E}_{\mathbf{h} \sim p_H(\mathbf{h})} P(\mathbf{h}|\mathbf{h})$ defined via the continuous $p_H(\mathbf{h})$ can be optimized using variational inference:

$$\begin{aligned} \log p_H(\mathbf{h}) &\geq \mathbb{E}_{\mathbf{h} \sim q_{\text{ord,cat}}(\cdot|\mathbf{h})} \left[\log p_H(\mathbf{h}) - \log q_{\text{ord,cat}}(\mathbf{h}|\mathbf{h}) + \log P(\mathbf{h}|\mathbf{h}) \right] \\ &= \mathbb{E}_{\mathbf{h} \sim q_{\text{ord,cat}}(\cdot|\mathbf{h})} \left[\log p_H(\mathbf{h}) - \log q_{\text{ord,cat}}(\mathbf{h}|\mathbf{h}) \right], \end{aligned}$$

for which we need a distribution $q_{\text{ord,cat}}(\mathbf{h}|\mathbf{h})$ that has support only where $P(\mathbf{h}|\mathbf{h}) = 1$. In other words, $q_{\text{ord,cat}}$ needs to be the probabilistic inverse of $P(\mathbf{h}|\mathbf{h})$, so the round and arg max functions.

So how do we ensure that $q_{\text{ord,cat}}$ is the probabilistic inverses of the round and argmax functions? For the ordinal data we construct a distribution as follows. First the variable \mathbf{u} is distributed as a Gaussian, $\mathbf{u}_{\text{logit}} \sim \mathcal{N}(\cdot | \mu(\mathbf{h}_{\text{ord}}), \sigma(\mathbf{h}_{\text{ord}}))$ where the mean and standard deviation are predicted by a shared EGNN (denoted by μ and σ) with the discrete features as input. Then $\mathbf{u} = \text{sigmoid}(\mathbf{u}_{\text{logit}})$ ensuring that $\mathbf{u} \in (0, 1)$. We will name this distribution $q(\mathbf{u}|\mathbf{h}_{\text{ord}})$. This construction is practical because we can compute $\log q_{\text{ord}}(\mathbf{u}|\mathbf{h}_{\text{ord}}) = \log \mathcal{N}(\mathbf{u}_{\text{logit}} | \mu(\mathbf{h}_{\text{ord}}), \sigma(\mathbf{h}_{\text{ord}})) - \log \text{sigmoid}'(\mathbf{u}_{\text{logit}})$ using the change of variables formula. Finally we let $\mathbf{h}_{\text{ord}} = \mathbf{h}_{\text{ord}} + \mathbf{u}$, for which we write the corresponding distribution as $q_{\text{ord}}(\mathbf{h}_{\text{ord}}|\mathbf{h}_{\text{ord}})$. This last step only shifts the distribution and so does not result in a volume change, so $\log q_{\text{ord}}(\mathbf{h}_{\text{ord}}|\mathbf{h}_{\text{ord}}) = \log q(\mathbf{u}|\mathbf{h}_{\text{ord}})$. Now since $\mathbf{u} \in (0, 1)$ we have that $\text{round}(\mathbf{h}_{\text{ord}}) = \text{round}(\mathbf{h}_{\text{ord}} + \mathbf{u}) = \mathbf{h}$ as desired.

For categorical data we similarly model a unconstrained noise variable $\mathbf{w} \sim \mathcal{N}(\cdot | \mu(\mathbf{h}_{\text{cat}}), \sigma(\mathbf{h}_{\text{ord}}))$ which is then transformed to respect the argmax constraint. Again, μ and σ are modelled by an EGNN. Let $i = \mathbf{h}_{\text{cat}}$, the index whos value needs to be the maximum and $\mathbf{w}_i = T$. Then $\mathbf{h}_{\text{cat},i} = T$ and $\mathbf{h}_{\text{cat},-i} = T - \text{softplus}(T - \mathbf{w}_{-i})$. Again the log-likelihood of the corresponding of the resulting distribution $q_{\text{cat}}(\mathbf{h}_{\text{cat}}|\mathbf{h}_{\text{cat}})$ is computed using the $\log \mathcal{N}(\mathbf{w} | \mu(\mathbf{h}_{\text{cat}}), \sigma(\mathbf{h}_{\text{ord}}))$ and the log derivatives of the softplus thresholding. For more details on these constructions see (Ho et al., 2019; Hoogeboom et al., 2021).